EVALUATION OF THE INERTIA FORCE IN COMPRESSIVE IMPACT LOADING ON STEEL FIBER-REINFORCED CONCRETE

Mohammad Bakhshi [(1)] [*], Isabel B. Valente [(1)], Honeyeh Ramezansefat [(1)] and Joaquim A.O. Barros [(1)]

[(1)] Department of Civil Engineering, Faculty of Engineering, University of Minho, Guimaraes, Portugal

[*] Corresponding author: Mohammad.bakhshi.ngd@gmail.com

ABSTRACT

Steel-fibre-reinforced concrete (SFRC) is a strain rate sensitive material and, therefore, its dynamic and static compressive behaviour can be significantly different. In the present study, the effect of loading rate on the compressive behaviour of SFRC with 1% hooked end steel fibres is experimentally investigated. During impact loading, an inertia force is created due to acceleration along the specimen, whose effect in the range of impact is studied for a comprehensive assessment of the dynamic analysis of SFRC structures. For the evaluation of the inertia force, an instrumented drop-weight test setup is used, which includes two fast response loadcells with capacities of 1000 and 2000 kN on top (impact force) and bottom (reaction force) of specimen. The drop-weight impact tests were performed with three different drop heights, corresponding to maximum strain rates that ranged from 1 to 50 s^{-1}. Two high-capacity accelerometers (5000 g) were mounted in the middle of the cylindrical specimens to obtain the cylinder acceleration response. The results show that, by increasing the strain rates, compressive strength, maximum acceleration at the middle of cylinder, and inertia force are increased. The results in terms of the ratio between inertia and impact load of specimens are presented and discussed.

KEYWORDS: Steel fiber reinforced concrete, drop-weight test, compressive strength, modulus of elasticity, inertia force, strain rate.

1. INTRODUCTION

Fibre reinforced concrete (FRC) has been widely used in the construction of high-rise buildings and critical protective structures, because adding fibres into the concrete matrix effectively increases the ductility and the impact energy absorption capacity of the structural elements and significantly improves the concrete´s cracking performance [1]. Steel fibre-reinforced concrete (SFRC) is more ductile and tough than plain concrete [2]. Steel fibres crossing cracks limit their propagation due to the mobilization of fibre pull-out mechanisms. Despite fibre reinforcement is mainly used to increase the post-cracking tensile behaviour of cement based materials, SFRC structural elements subjected to impact have significant zones under pronounced compressive stress field, whose sensitivity to high strain rates is important to access for a comprehensive modelling if its behaviour.. Bischoff and Perry [3] investigated the effect of strain rate on the compressive behaviour of plain concrete by performing

different test procedures to determine its dynamic characteristics and concluded that the properties of concrete under dynamic and static loading are different.

The majority of the research developed on the dynamic material properties of SFRC is based on experimental tests and several experimental techniques have been developed for investigating the mechanical properties of concrete under impact loading. Figure 1 suggests the test method to be adopted for the desired loading rate (with a correspondence on the strain rate). The impact loadings can be applied by non-instrumented multiple drop weight, weighted pendulum (Charpy), instrumented drop weight, Split-Hopkinson Pressure Bar (SPHB), and projectile, [4].

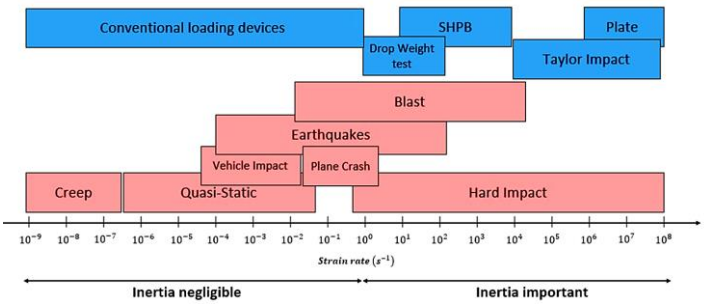

Figure 1. Categorize of loadings based on the strain rate regime, [5].

Several factors affect the strain rate sensitivity of SFRC, including compressive strength, type of loading (i.e., compressive, tensile, and flexural), temperature, and type of steel fibres [6,7]. Generally, the effect of strain rate on the mechanical properties of concrete is represented by the dynamic increase factor (DIF), which is defined as the ratio of dynamic to static values of the certain property. The effect of strain rate on the mechanical behaviour of SFRC has been investigated by different researchers [3, 8, 9]. Wang *et al.* [9] performed some compressive tests on plain concrete and SFRC specimens with three different volume fractions of very short straight steel fibres (1.5%, 3% and 6%). The results showed that the compressive strength of SFRC increased with both the strain rate and the volume fraction of steel fibres. Lok and Zhao [8] investigated the dynamic compressive behaviour of SFRC with hooked end fibres, using the SHPB test. They found that the compressive strength of SFRC increased with the strain-rate. Although there is no standard test for SFRC cylinders under compressive impact loading, instrumented drop weight tests were carried out by Xu *et al.* [6] on standard SFRC cylinders to study their compressive behaviour under impact loading. These authors used synthetic fibres, undulated, cold rolled, flattened, hooked end, and two new spiral shape steel fibres in their experimental study. They showed that the rate sensitivity and material properties of FRC under compressive impact loading are dependent on the material type and on the shape of fibres. Regarding the dynamic compressive behaviour of SFRC, many researchers consider the compressive dynamic increase factor (DIF) as a principal parameter [2, 7, 9]. Banthia [2] studied the effect of inertia force in SFRC beams under impact loading using an instrumented drop weight test. He reported that, for evaluating the flexural behaviour of the beam, due to inertia force in the impact loading, the reaction forces must be used instead of the contact load between the hammer and the beam. The recorded impact load of hammer can be corrected if the acceleration distribution along the length of the beam is known. Three accelerometers were used in his study for this purpose.

In the present study, the variation of the inertia force, at different strain rates, was investigated. For that purpose, acceleration was measured at the middle of SFRC cylindrical specimens. The relationship between inertia force, impact load and strain rate are determined and discussed. Moreover, the effect of strain rate on compressive strength and modulus of elasticity of SFRC is investigated. The developed

SFRC mixture includes 1% volume fraction of hooked end steel fibres with length of 30 mm and aspect ratio of 80. This hooked end fibre was used due to its relatively high reinforcement performance, demonstrated in several experimental works. An instrumented drop-weight impact test setup is designed for the experimental analysis. Drop-weight impact tests are performed with four different drop heights, corresponding to maximum strain rates ranging from 1 to 50 s^{-1}. At least three cylindrical specimens are tested for each rate of loading and each height of the impactor.

2. EXPERIMENTAL PROCEDURE

2.1. Materials

A single type of SFRC was used throughout the experiments, made with EN 197-1 [10] type I cement, 42.5R with a specific density of 3.15 gr/cm^3, and fly ash Type II according to EN 450-1 [11] requirements. Normal-weight natural river fine and coarse aggregates were used, with saturated-surface-dry (SSD) densities of 2.60 and 2.64 g/cm^3, respectively, and maximum size of 12 mm. The superplasticizer SIKA ViscoCrete 5920 was used. The content of each ingredient of the SFRC mixture presented in Table 1 was obtained by applying the volume method recommended by ACI-544-1R [12]. The geometric and mechanical properties of the used hooked-end steel fibres are indicated in Table 2.

Table 1. Mix proportion of SFRC in one m^3.

Cement [kg]	Fly ash [kg]	Water-cement content ratio	Fine aggregate [kg]	Coarse aggregate [kg]	Superplasticizer [kg]	Steel fiber [kg]
400	200	0.3	942	628	4.8	75.8

Table 2. Properties and amount of utilized steel fibre.

Volume [%]	Mass [kg/m^3]	Diameter [mm]	Length [mm]	l/d	Modulus of elasticity [GPa]	Tensile strength [MPa]
1	75.8	0.38	30	80	210	2300

2.2. Static tests

Quasi-static loading tests were conducted in cylindrical specimens of 100 mm diameter and 200 mm height to evaluate the compressive strength and modulus of elasticity according to EN 12390-2 [13]. These tests were executed in a servo-hydraulic testing machine with a maximum load capacity of 3000 kN, and three strain gauges were used to measure the compressive strain.

2.3. Impact tests

The instrumented drop-weight system used in the compressive tests was developed to apply compressive impact loads with varying heights and masses, as shown in Figure 2a. It has the capacity to drop a maximum mass of 290 kg up to a height of 9 m, which corresponds to a theoretical maximum impact velocity of 13.3 m/s. The inertia force is calculated from the difference between the forces measured on top and bottom of the specimens. The two accelerometers are installed with 90-degree radial distance, in the backside of the cylinders in the view of camera position, Figure 2b. The recording rate capacity of this control card is 50 samples per millisecond, when multiple channels are used simultaneously, and results show that the recording rate was sufficient. The failure process, crack velocity, and deformation of specimens were measured with a high-speed video camera. These measurements were used to calculate strain values and strain rates in the tested specimens, during the impact loading process. The strain and the strain rates were also directly measured by three strain gauges installed at the specimen's mid height.

(a) (b)

Figure 2. (a) The drop weight impact machine and (b) Cylinders under impact test.

Two approaches were considered for measuring the deformation of the specimens. In the first approach, a PHOTRON FastCam APX-RS (PHOTRON, Japan) with the capability of recording up to 50,000 frames per second (fps) to measure surface deformations of cylindrical specimens ignoring the effect of curvature, was used, together with halogen lights that were installed to provide the lighting required for the high-speed videos. In the present experimental study, the high-speed camera was able to record the impact process with a rate of 15,000 frames per second and a resolution of 128×256 pixels, Figure 3. The recorded videos were analysed by GOM Correlate software for digital image correlation (DIC).

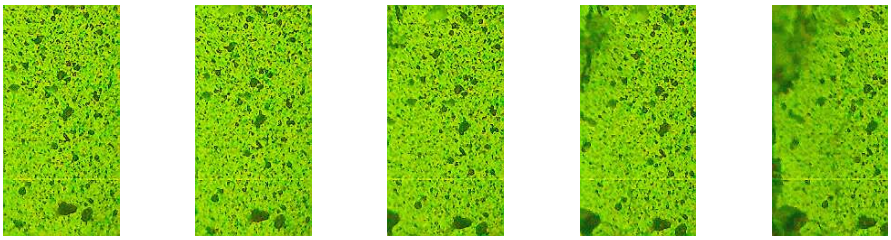

0.000 ms 0.353 ms 0.706 ms 0.971 ms 1.324 ms

Figure 3. Typical test sequence for SFRC recorded with High-speed camera (specimen HS2-2).

In the second approach, the hammer velocity during the impact period ($\dot{\delta}(t)$) was obtained through the initial impact velocity and the integral of the acceleration recorded by the accelerometer ($\ddot{\delta}(t)$). Subsequently, average compressive deformability ($\delta(t)$) was determined by the integral of the velocity.

$$\dot{\delta}(t) = \int \ddot{\delta}(t)dt \quad (1)$$

$$\delta(t) = \int \dot{\delta}(t)dt \quad (2)$$

deformability at the middle of cylinder height, respectively. In total, 16 cylinders were tested with four different heights of impactor of 1000 (HS1), 1500 (HS2), 2000 (HS3), and 2500 mm (HS4), corresponding to contact velocities of 4.42, 5.42, 6.26, and 7.00 m/s, respectively. These different heights were considered in order to determine the effect of the strain rate on the compressive strength and modulus of elasticity, and also to evaluate the variation obtained on inertia force and maximum acceleration.

The deformation along the height of cylinder is obtained with the high-speed camera that records the deformation in the middle of the cylinder surface, in a frame with 70 mm height and 5 mm width. The data collected also shows that the deformation distribution can be assumed linear along the height of cylinder. Similar results were reported by other researchers [14]. To evaluate the variation of acceleration along the height of cylinders, eight different points were defined. Afterwards, the acceleration was consecutively measured in these eight points, with two accelerometers, in specimens tested with an impactor of 20 kg, dropping from a height of 10 cm. The results show a non-uniform axial acceleration along the height of the cylinder, as presented in Figure 4. Considering the trend presented in Figure 4, it was assumed that the acceleration distribution along the axial direction of the specimen decreases linearly from the top to the bottom, as is also shown in Figure 4. Based on the deformation and acceleration distribution along the height of the cylinder, maximum acceleration at the middle of cylinder is selected as an average acceleration. Regarding the maximum acceleration values measured in the specimen, during impact loading, two values of acceleration are considered: (a) the maximum acceleration at the middle of cylinder height measured by two accelerometers ($\ddot{\delta}_{mid}$), and (b) the maximum acceleration in the contact point between impactor and cylinder at the highest point of specimen ($\ddot{\delta}_{top}$) that is two times of its middle value, if a linear axial distribution is assumed.

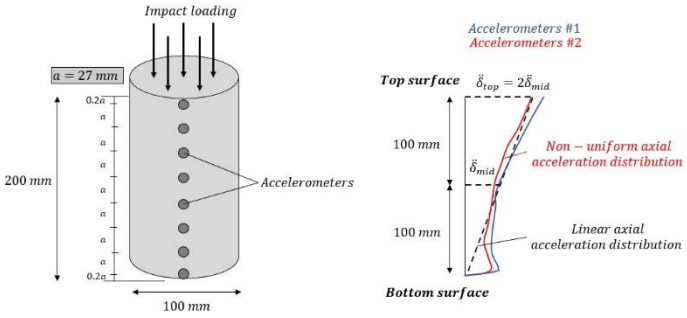

Figure 4. Assumed acceleration distribution.

A linear variation of deformation from the top to the bottom of the specimen, and also a linear variation on the values of velocity ($\dot{\delta}$) and acceleration ($\ddot{\delta}$) is assumed, Figure 5. It means that the acceleration distribution follows the deformation distribution along the height of specimen [2] in the time step, for a given time increment of Δt, ($\Delta t = t_2 - t_1$).

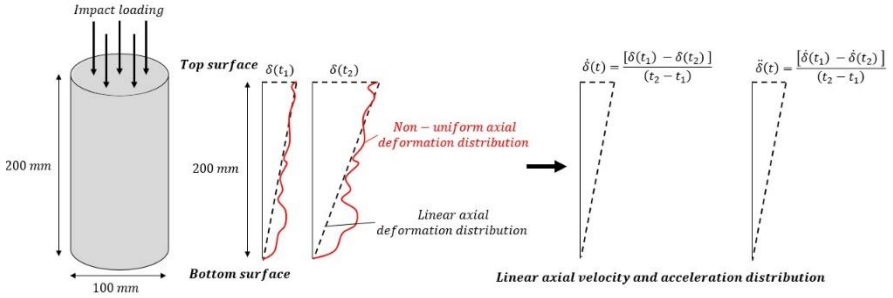

Figure 5. Assumed deformation, velocity, and acceleration linear distribution.

3. RESULTS AND DISCUSSION

3.1. Failure patterns and fracture surfaces

In the specimens tested under static loading, micro cracks propagate mainly parallel to the direction of loading. For this loading situation, cracks progressed roughly in the axial direction of the specimen and a cone-shape failure was observed (Figure 6a).

Under impact loading, a large number of cracks were formed and then propagated along the cylinders. By increasing the height of the impactor, an increase in the number of fractured pieces was observed in the tested specimens, showing the effect of strain rate on the failure of SFRC cylinders (Figure 6b to Figure 6e). The increase in the number of fractured pieces is an indication of a higher energy dissipation capacity of the specimen. Moreover, pull-out was the dominant mechanism for hooked end fibres in SFRC cylinders tested in this series. The cone-shape failure was also observed under impact loading, with more fractured pieces than under static loading. By increasing the height of impactor, the number of fractured pieces has increased. It means that by increasing the height of impactor, the energy absorption capacity of cylinder under impact loading increases.

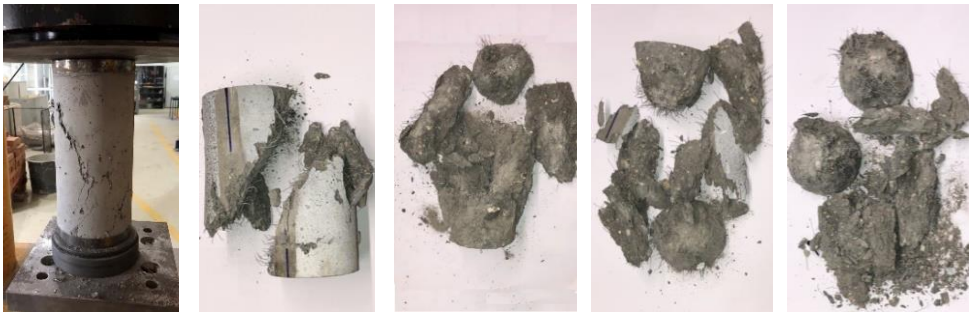

a) Static b) Impact (1.0 m) c) Impact (1.5 m) d) Impact (2.0 m) e) Impact (2.5 m)

Figure 6. Failure modes of SFRC cylinders under static and impact loading.

3.2. Mechanical properties

The mechanical properties of specimens tested under static and impact loading are shown in Table 3. The strain rate for the static compressive test is 1.33E-05. For all cylindrical specimens, the strain at compressive strength is almost 2.4‰. In normal concrete, this value ranges between 2.0‰ to 2.3‰. In impact loading, as expected, the strain rate influences the compressive strength and peak strain, and modulus of elasticity of SFRC. Both the compressive strength and modulus of elasticity have increased with the strain rate. The log-linear graph is used to represent the relationship between DIF and strain rate. It was observed that the values of DIF-*E* (modulus of elasticity) are higher than the values of DIF-f_c (compressive strength).

The results obtained are also compared with the models proposed by CEB-FIP [15,16] to predict the modulus of elasticity and the compressive strength as a function of the strain rate. In the SFRC, the DIF-f_c has ranged between 1.04 and 1.35, while the DIF-*E* has varied between 1.22 and 1.58. For both compressive strength and modulus of elasticity, the CEB-FIP model overestimates the DIF up to strain values around $30s^{-1}$. For strain rates higher than $30s^{-1}$, the obtained compressive strengths are in good agreement with the values predicted by the CEB-FIP models. When the strain rate is higher than 30 s^{-1}, the CEB-FIP model underestimates the value of DIF-*E*, Figure 7.

Table 3. Influence of strain rate on the mechanical properties of SFRC.

Type ID	Strain rate [s^{-1}]	Top load [kN]	Bottom load [kN]	Modulus of elasticity (E) [GPa]	DIF-E	Compressive strength (f_c) [MPa]	DIF-f_c
S-1	1.33E-05	585.0	nr	41.72		73.07	
S-2	1.33E-05	601.9	nr	42.40	1.000	76.72	1.000
S-3	1.33E-05	529.0	nr	40.55		67.09	
HS1-1	10.80	634.1	585.3	50.69	1.220	74.56	1.023
HS1-2	8.39	636.6	589.4	49.34	1.187	75.08	1.031
HS1-3	9.41	636.9	602.3	53.71	1.293	76.73	1.053
HS1-4	10.15	681.8	619.3	54.13	1.303	78.89	1.083
HS2-1	18.65	nr	610.7	61.40	1.478	77.80	1.068
HS2-2	25.18	700.2	626.8	59.63	1.435	79.85	1.096
HS2-3	19.50	685.7	632.6	52.40	1.261	80.59	1.106
HS2-4	21.22	673.4	613.1	56.54	1.361	78.10	1.072
HS3-1	29.28	795.8	640.2	59.26	1.426	81.55	1.119
HS3-2	36.17	861.4	702.4	63.29	1.523	89.48	1.228
HS3-3	34.60	852.9	649.3	65.46	1.575	82.71	1.135
HS3-4	24.65	nr	688.7	64.12	1.543	87.73	1.204
HS4-1	27.27	1052.0	716.6	60.91	1.466	91.29	1.253
HS4-2*	41.34	nr	1123.2	67.77	1.631	143.08	1.964
HS4-3	37.94	nr	755.7	61.47	1.479	96.27	1.321
HS4-4	35.83	nr	742.6	63.26	1.523	94.60	1.299
HS4-5	39.21	nr	769.1	60.53	1.457	97.97	1.345

nr – not recorded

* The results obtained with specimen HS4-2 are considered as outliers

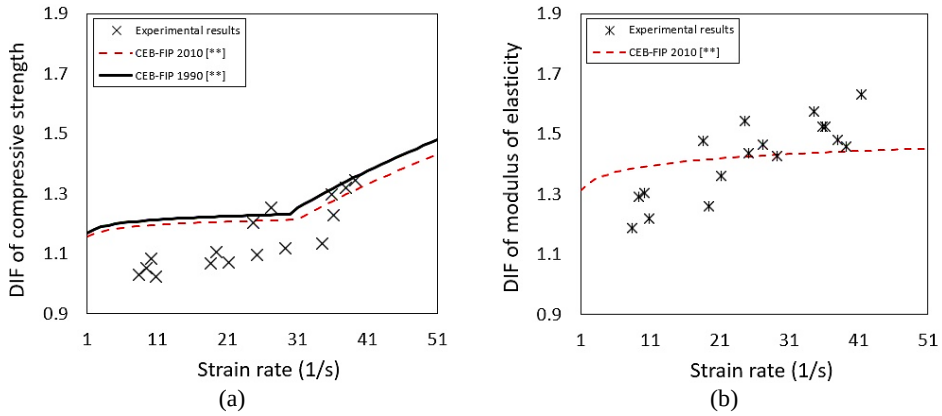

Figure 7. DIF of SFRC for (a) compressive strength and (b) modulus of elasticity.

3.3. Effect of inertia in impact loading

Figure 8 shows the values of impact and reaction forces along time (top load in three of the tested specimens could not be measured due to load cell limitations). The time intervals between the starting moment of the impact force and the reaction force are 134, 121, 99 and 80 μs, corresponding to drop heights of 1000, 1500, 2000, and 2500 mm, respectively. Therefore, increasing the height of impactor

provokes an increase in impact and reaction forces, while the time gap between impact and reaction decreases. The time delay between top and bottom load cells and strain gauges installed at the mid height of cylinders can be attributed to stress wave propagation along the specimens. Based on these results, the forces recorded by top and bottom load cells show different values under impact loading, which means that the inertia force is significant. As it is known, the value of inertia force is a function of the acceleration along the specimen. The test results indicate that the ratio between inertia force and impact force (recorded by top load cell) significantly depends on the acceleration. This observation is also reported by Xu *et al.* [6]. The accelerations are measured by two accelerometers positioned at the mid height of specimens. The results indicate that by increasing the height of impactor, the acceleration increases and, accordingly, the value of inertia force also increases. For impactor heights of 1000, 1500, 2000, and 2500 mm, the maximum acceleration values are 1013g, 1487g, 1611g, and 3173g, respectively, and the ratio of inertia force to impact force (ω) is 9%, 10%, 24%, and 32%, respectively, as presented in Table 4. In the present study, to eliminate the inertia effect on the material properties, the reaction force measured by the bottom load cell is considered for calculating the compressive strength of SFRC under impact loading.

Table 4. Effect of strain rate on maximum acceleration and inertia force.

Type ID	Strain rate $[s^{-1}]$	m [kg]	Impact force [kN]	Inertia force [kN]	Inertia to impact force ratio (ω)	$\ddot{\delta}_{max,mid}$ [g*]	$\ddot{\delta}_{max,top}$ [g*]	$m\ddot{\delta}_{max,mid}$ [kN]	$m\ddot{\delta}_{max,top}$ [kN]
HS1-1	10.80	3.63	634.1	48.8	0.077	831	1662	30.1	60.3
HS1-2	8.39	3.75	636.6	47.2	0.074	987	1974	37.0	74.0
HS1-3	9.41	3.71	636.9	34.6	0.054	741	1482	27.5	55.0
HS1-4	10.15	3.61	681.8	62.5	0.092	1013	2026	36.6	73.2
HS2-1	18.65	3.75	nr	nr	nr	nr	nr	nr	nr
HS2-2	25.18	3.68	700.2	73.4	0.105	1487	2974	54.7	109.4
HS2-3	19.50	3.72	685.7	53.1	0.077	1339	2678	49.8	99.7
HS2-4	21.22	3.75	673.4	60.3	0.090	1270	2540	47.7	95.3
HS3-1	29.28	3.61	795.8	155.6	0.196	1574	3148	56.8	113.7
HS3-2	36.17	3.72	861.4	159	0.185	1509	3018	56.1	112.2
HS3-3	34.60	3.73	852.9	203.6	0.239	1611	3222	60.1	120.1
HS3-4	24.65	3.72	nr	nr	nr	1690	3380	62.8	125.7
HS4-1	27.27	3.74	1052.0	335.4	0.319	3173	6346	118.6	237.1
HS4-3	37.94	3.74	nr	nr	nr	2064	4128	77.2	154.3
HS4-4	35.83	3.64	nr	nr	nr	2878	5756	104.7	209.3
HS4-5	39.21	3.66	nr	nr	nr	3118	6236	11.4	22.9

nr – not recorded

* g=9.81 $m.s^{-2}$

The inertia force can be analytically calculated by the equation of motion. According to structural dynamic theory, when an element moves relative to a reference, the inertia forces are proportional to the value of its acceleration in the same direction [17]. Consequently, by increasing the amount of created acceleration, the inertia force is increased. The motion equation can be written for a cylinder under impact loading. Based on this equation, the inertia force is a function of the specimen's mass and acceleration, as defined in Equation (3),

$$\sum F = F_i = F_t - F_b = m\ddot{\delta}_{max} \tag{3}$$

where F_i, F_t, F_b, m, and $\ddot{\delta}_{max}$ are the inertia force, impact load (top), reaction load (bottom), mass of specimen, and maximum acceleration, respectively. In the compressive impact test (instrumented drop weight test), the specimen (motion of particles) is constrained to deform in the loading direction, and therefore, only the inertia load in the loading direction is calculated. For evaluating the relationship between maximum acceleration and inertia force, both the maximum acceleration at the middle of the cylinder height ($\ddot{\delta}_{max,mid}$) and the maximum acceleration in the contact point of impactor and cylinder ($\ddot{\delta}_{max,top} = 2\ddot{\delta}_{max,mid}$) are considered, as an input to the equation of motion, Figure 8a.

. The analytical inertia force is calculated based on the assumption of linearity distribution of acceleration along the height of cylinder. When the calculated analytical inertia force is compared with the experimental inertia force, it can be observed that when the loading rate (or height of impactor) increases, the analytical equation further underestimates the inertia force, Figure 8a. This may be attributed to the real non-linear distribution of acceleration along the height of the cylinder. By increasing the contact velocity (or height of the impactor), the non-linearity of the acceleration distribution increases. It means that in the higher contact velocity, the maximum acceleration is dependent not only on the contact velocity but also on the height of the cylinder. Afterward, when the non-linearity of the acceleration distribution increases, the assumption of linearity for acceleration distribution could not be completely satisfied. Therefore, the value of the inertia force obtained by the equation of motion must be modified, assuming a non-linear distribution along the height of the cylinder. Further experimental tests are needed to confirm this hypothesis. In addition, the inertia to impact force ratio also increases when the maximum acceleration is increased, in an approximately linear trend, Figure 8b. By increasing the height of the impactor, the effect of inertia is more significant. Similar observations have also been reported in [2] and [6].

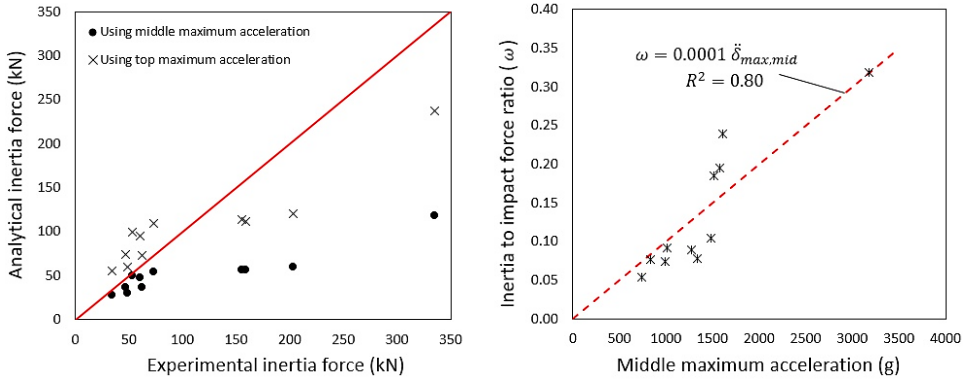

Figure 8. Comparison between: (a) experimental and analytical inertia force, (b) inertia to impact force ratio and maximum acceleration in the middle of the specimen.

4. CONCLUSION

This paper investigates the effect of strain rate on the compressive behaviour of SFRC and analyses the parameters of compressive strength and modulus of elasticity. It also investigates the effect of inertia force in the compressive impact loading of hooked end SFRC and its relationship with maximum acceleration measured in cylindrical specimens. The following conclusions are reached:

1- Compressive strength and modulus of elasticity of SFRC increase with the strain rate. For the highest strain rate tested, maximum DIF values of 1.35 and 1.58 were obtained for compressive strength and modulus of elasticity, respectively.

2- The maximum acceleration value at the middle of the cylinder has increased with the strain rate. Consequently, the inertia force has also increased. The difference between analytical and experimental inertia forces has increased with the strain rate. It is concluded that a non-linear distribution of acceleration is likely, and the linear distribution assumption is not valid for all ranges of strain rate.

ACKNOWLEDGEMENTS

The study reported in this paper is part of the project “PufProtec - Prefabricated Urban Furniture Made by Advanced Materials for Protecting Public Built” with the reference of (POCI-01-0145-FEDER-028256) supported by FEDER and FCT funds. The first author gratefully acknowledges the financial support of FCT-Fundação para a Ciência e Tecnologia for the Ph.D. Grant SFRH/BD/149246/2019.

REFERENCES

[1] Barros, J. A., Cunha, V. M., Ribeiro, A. F., & Antunes, J. A. B., 'Post-cracking behaviour of steel fibre reinforced concrete', *Materials and Structures*, 38(1) (2005) 47-56.

[2] Banthia, N., & Mindess, S., 'Impact resistance of steel fiber reinforced concrete', *Materials Journal*, 93(5) (1996) 472-479.

[3] Bischoff, P. H., & Perry, S. H., 'Compressive behaviour of concrete at high strain rates', *Materials and structures*, 24(6) (1991) 425-450.

[4] Wu, H., Fang, Q., Gong, J., Liu, J. Z., Zhang, J. H., & Gong, Z. M., 'Projectile impact resistance of corundum aggregated UHP-SFRC', *Int. Journal of Impact Engineering*, 84 (2015) 38-53.

[5] Nyström, U., & Gylltoft, K., 'Numerical studies of the combined effects of blast and fragment loading', *International Journal of Impact Engineering*, 36(8) (2009) 995-1005.

[6] Xu, Z., Hao, H., & Li, H. N., 'Experimental study of dynamic compressive properties of fibre reinforced concrete material with different fibres', *Materials & Design*, 33 (2012) 42-55.

[7] Othman, H., Marzouk, H., & Sherif, M., 'Effects of variations in compressive strength and fibre content on dynamic properties of ultra-high-performance fibre-reinforced concrete', *Construction and Building Materials*, 195 (2019) 547-556.

[8] Lok, T. S., & Zhao, P. J., 'Impact response of steel fiber-reinforced concrete using a split Hopkinson pressure bar', *Journal of Materials in Civil Engineering*, 16(1) (2004) 54-59.

[9] Wang, S., Zhang, M. H., & Quek, S. T., 'Effect of high strain rate loading on compressive behaviour of fibre-reinforced high-strength concrete', *Magazine of concrete research*, 63(11) (2011) 813-827.

[10] British Standard Institution, BS EN 197-1, 'Cement Composition, specifications and conformity criteria for common cements', *BSI London* (2011).

[11] British Standard Institution, BS EN 450-1, 'Fly ash for concrete Definition, specifications and conformity criteria', *BSI London* (2012).

[12] ACI 544.1 R-96, 'State-of-the-Art Report on Fiber Reinforced Concrete', *ACI Committee*, (1996).

[13] British Standards Institution, BS EN 12390-2, 'Testing hardened concrete Making and curing specimens for strength tests', *BSI London* (2009).

[14] Mindess, S., & Zhang, L., 'Impact resistance of fibre-reinforced concrete', *Proceedings of the Institution of Civil Engineers-Structures and Buildings*, 162(1) (2009) 69-76.

[15] CEB-FIP, C., 'Model code 2010', *Comite Euro-International du beton* (2010).

[16] CEB-FIP, C., 'Design code', *Comite Euro International du beton*, (1990) 51-59.

[17] Craig Jr, R., & Kurdila, A. J., 'Fundamentals of structural dynamics, *John Wiley & Sons*, (2006).